ICAS 2021 SHANGHAI
International Council of the Aeronautical Sciences
32nd Congress of the International Council of the Aeronautical Sciences
September 6-10, 2021
Pudong Shangri-La, Shanghai, China

STATIC AEROELASTIC TAILORING OF A HIGH-ASPECT-RATIO-WING FOR A SAILPLANE WITH A FORWARD MORPHING WING SECTION

Fabian Sturm[1], Gerrit Illenberger[1], David Techmer[1] & Mirko Hornung[1]

[1]Institute of Aircraft Design,Technical University of Munich

Abstract

A sailplane with a morphing forward wing section allows a promising increase in performance. As a consequence, the morphing forward section leads to a smaller primary structure and reduced torsional stiffness. As the shear center is moved aft the aerodynamic center, an aeroelastic twisting moment is induced on the high-aspect-ratio wing. The layup and fiber angles of the wing shells are optimized to counteract the adverse wing twist by modifying stiffness and applying bending-torsion-coupling. An efficient parametrization and optimization method of the wing skin layup is developed for a finite element shell model of the wing structure. The aerodynamic model utilizes a doublet lattice model, based on an optimized aerodynamic wing design for a morphing wing sailplane. Structural masses and masses for controls, flaps and water ballast are included with discrete mass elements. To solve the static aeroelastic problem and to determine the deflection, NASTRAN `SOL144` is used. Load cases for low- and high speed conditions as well as for pull-up manoeuvres are analyzed. Results show that the bending-torsion-coupling effect can have a beneficial or adverse effect depending on the specific load case and aerodynamic configuration.

Keywords: sailplane, morphing wing, morphing structure, aeroelastic tailoring

Nomenclature

Symbols

c_l	lift coefficient, airfoil
C_L	lift coefficient, aircraft
lb	lower bound
m	mass, kg
n_z	aircraft load factor
t	thickness, mm
u	nodal displacement, mm
ub	upper bound
ur	nodal rotation, °
v	airspeed, km/h
$\vec{x}$	design variable vector
$z(\vec{x})$	objective function
x, y, z	wing coordinate system, mm
θ	wing twist angle, °
ϕ	fiber orientation angle, °
γ	local wing dihedral angle, °

Subscripts

CG	center of gravity
i	index design variables
j	index wing nodes
k	index load cases
NL	non-lift
S	structure
WB	water ballast

Abbreviations

CFRP	carbon fiber reinforced plastics
CLT	classical laminate theory
DLM	doublet lattice method
FEM	finite element method
HM	high modulus
HT	high tenacity
LC	load case
LE	leading edge
MC	mass configuration
MTOM	maximum take-off mass
TE	trailing edge
UD	unidirectional

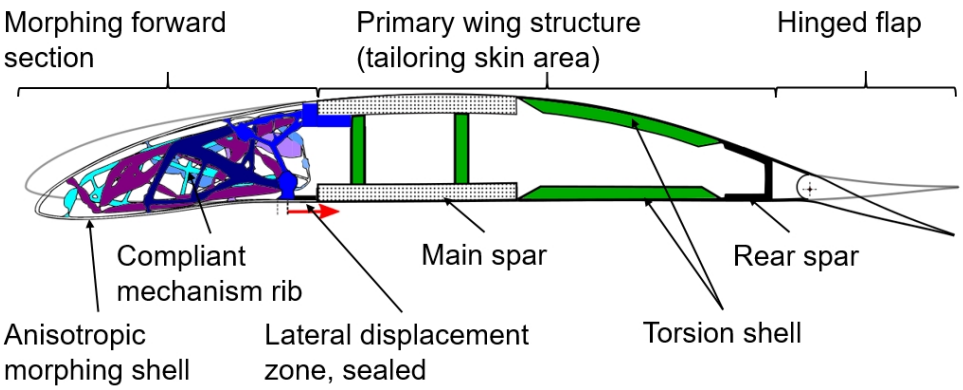

Figure 1 – Structural concept of wing with morphing forward section.

1. Introduction

Sailplanes operate in a broad range of speeds, from low speed circling in thermals to high cruising speeds for a maximum average flying speed. The objective is, to operate within the laminar-low-drag-bucket for the whole range of lift coefficients to achieve high lift-to-drag-ratios. State of the art is the application of hinged trailing-edge flaps for lift coefficients from C_L = 0.2 to C_L = 1.5. A combination with a morphing forward section allows airfoils with higher lift coefficients while maintaining large extends of laminar flow [23]. Achleitner optimized airfoils and a wing planform for that application with a maximum lift coefficient of up to C_L = 1.8 [1]. This concept allows to reduce the wing area and increase the wing loading while maintaining the same low-speed performance. As a result, the wetted wing area and absolute profile drag is reduced, which leads to higher lift-to-drag-ratios at higher speeds. The wing comprises a morphing forward section of 25% chord length, the primary structure which includes the wing spar and the torsion cell, and a hinged trailing edge flap as shown in figure 1. With a span of 18 m, a high aspect ratio of 37 is achieved.
A target airfoil displacement is imposed on the flexible, anisotropic shell by elastic ribs that are composed of compliant mechanisms, to switch between distinct airfoil shapes [20], [17]. As the morphing shell can move laterally in chordwise direction on the lower side, its contribution to the total torsional stiffness of the wing is low. The reduced torsion cell area requires a higher material stiffness to maintain the desired torsional stiffness. As the shear center of the reduced wing structure is moved aft, compared to a conventional design, and is behind the aerodynamic center of the airfoils, lift leads to a twisting moment. It is superimposed with an airfoil pitching moment. This aeroelastic twist can lead to an adverse aerodynamic performance and shall be avoided. A preliminary structural and aerodynamic model of a previous aerodynamic design of a morphing wing sailplane has been analyzed and optimized by Schlothauer [18]. He developed an optimization approach to minimize wing twist and spar cap stress with a FE model and uncoupled aerodynamic loads. An improved aerodynamic and structural design of the concept has been analyzed with NASTRAN by Illenberger [10]. It could be shown that the adverse wing twist can be reduced by creating a specific bending-torsion-coupling with a mirrored cross-ply laminate. The objective is to reduce aeroelastic twist along the wingspan for specific load cases. Design variables are fiber angles and composite layup thicknesses of the wing shell. A static aeroelastic analysis provides the system responses. The modelling approaches for the elastic structure, masses and aerodynamics are shown. Also the solution method and optimization setup are described.

2. Aeroelastic Tailoring

Aeroelastic Tailoring is the optimization of structural stiffness of a wing that is subjected to aerodynamic load and elastic deformation. Usually elastic coupling effects within the structure are utilized. Shirk et al [19] gave an overview over the various objectives and principles of aeroelastic tailoring on aircraft. A laminate stiffness optimization of a wing that leads to a nose-down twist (wash-out) can be beneficial for maneuver drag reduction, maneuver load relief and divergence prevention. A nose-up twist (wash-in) characteristic is beneficial for lift effectiveness, control effectiveness and flut-

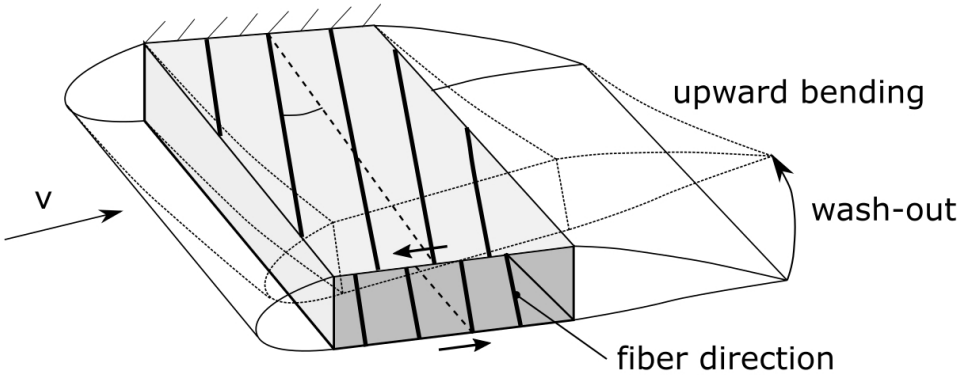

Figure 2 – Bending-twist coupling of a generic wing with an unbalanced, mirrored skin laminate.

ter prevention. The application of aeroelastic twist-coupling effects on rotor blades of horizontal axis wind turbines has been investigated by Lobitz et al [13]. The objectives reach from improved energy capture to load mitigation.
According to Shirk [19], selected directional stiffness is used to control elastic deformation under aerodynamic load in a beneficial way. Means to control directional stiffness can be selected fiber angles in a composite structure that make use of the orthotropic material properties. Hereby a coupling of bending and torsion deformation can be achieved. If the primary stiffness direction is moved forward of the elastic axis, a wash-out can be achieved, so a positive wing bending leads to a nose-down twist. Karaolis et al [12] investigated aeroelastic behavior of wind turbine blades and showed that a composite layup with unbalanced fiber angles in the turbine skins can be utilized for two types of twist coupling. The mirror-type layup with parallel fiber orientation on the upper and lower skin leads to bending-twist coupling and the helical layup with constant fiber orientation along the circumference of the wing hull leads to tension-twist coupling. The principle of bending-torsion coupling is shown in figure 2 for an unbalanced and mirrored UD laminate. The effect is achieved by the opposite stress situation on the upper and lower wing side. For a positive aircraft load factor with upward wing bending, there is compression stress in the upper wing shell and tension stress in the lower shell. An unbalanced laminate with respect to the wing's elastic axis will shear forward on the upper wing side and shear backwards on the lower side, leading to a wash-out twist. This can be achieved by mirrored UD plies or cross-ply laminates that are rotated in a range between 0 ° and 90 °. The effect will be dominated by the plies with the highest tensile stiffness in spanwise direction in the case of laminates with more than one fiber direction, thickness or material. So in the case of a 90 ° cross-ply laminate, the fibers oriented with the smaller angle to the elastic axis contributes most to the coupling effect. Usually to achieve the highest torsional stiffness and to avoid any coupling an angle of 45 ° is chosen as a conventional shell laminate. The maximum coupling is achieved at an angle of 22.5 °, considering the orthotropy of a 90 ° cross-ply laminate.

With regard to numerical optimization of composite stiffnesses, the challenge of parametrization arises, as there can be a high number of design variables. In general some of them are continuous, some are discrete, like ply thickness. Vanderplaats [22] showed numerical optimization methods for composites in general and specifically for Aeroelastic Tailoring of aircraft wings. Laminate thickness was treated as a continuous variable first and rounded to the next available ply thickness afterwards. IJsselmuiden [9] investigated design and optimization of variable stiffness laminates by means of changing ply angles, thicknesses and stacking sequences. The large number of continuous and discrete design variables and constraints leads to a non-convex design space with multiple solutions. On a large structure several laminates can be used, which enlarges the optimization problem. Here, fiber continuity and manufacturability have to be considered. IJsselmuiden separated the problem into a design requirement problem with stiffness optimization and a manufacturing requirement problem to determine actual laminate parameters like ply angles and thicknesses.
A conservative convex separable approximation was developed, that uses CLT stiffness matrix terms

instead of laminate parameters, which minimizes the number of design variables and leads to a convex problem. Strength and buckling behavior however depend also on stacking sequence in general. Dillinger [5] presented different methods for numerical optimization of variable-stiffness composite wing structures to minimize weight or maximize aileron effectiveness. The wing is represented by a number of design fields, each one with a stiffness matrix and thickness. A gradient based optimizer, that requires sensitivities from FEM, was used by IJsselmuiden [9]. In [6] he investigated aerodynamic corrections in static aeroelastic optimization. Laminate stiffnesses and thicknesses are used as design variables that are internally transformed to lamination parameters. So it is possible to formulate a continuous and convex optimization problem. Strength, buckling, mass, aileron effectiveness, divergence and twist were considered as responses. Dillinger was also involved in optimizing the aeroelastic behavior of the high-performance open class sailplane 'Concordia' with a span of 28 m and an aspect-ratio of 57.3 [3], [4]. An unbalanced layup was used with the objective to minimize wing twist for all relevant flight conditions for maximum aerodynamic performance at maximum take-off mass. Van den Bosch [21] used sectional stiffness data of a sailplane aileron structure to model it with beam elements. The objective of the ply angle optimization was to minimize aileron twist from wing bending for several load cases. Also pre-twisting the structure was investigated.

3. Technical Approach

3.1 Prerequisites and Assumptions

A sailplane wing structure is composed of two main load bearing components, each with a primary function. The main spar, usually an I- or box-beam, transfers the vast majority of bending and shear loads from lift, whereas the shell transfers shear loads from torsional moments. To keep the cross section closed for a high torsional stiffness, upper and lower wing shell are bonded with an omega- or c-shaped rear spar and a bonded, stiff nose. The contribution of the morphing forward section to torsional stiffness is low due to the layup and the structural slit on the lower side.

Sailplanes extract energy from the atmosphere. This allows to achieve performance benefits with a higher take-off mass in sufficiently strong updrafts, in contrast to motor-powered aircraft where a high take-off mass is disadvantageous. To achieve high lift-to-drag ratios at high airspeeds even additional water ballast is loaded into sailplanes. Though, there is limit for maximum structural mass. A maximum stall speed of 80 km/h without water ballast has to be achieved to fulfill the certification requirements [7]. For a given aerodynamic configuration and sailplane category, this defines the upper limit of structural mass.

Crucial for maximum performance is to achieve the designed aerodynamic geometry. The airfoils have to operate within the laminar-low-drag-bucket and therefore within a certain angle of attack range to avoid increased profile drag. The lift over span has to be distributed for minimum induced drag by the desired local airfoil lift coefficients. Deviations from the designed wing twist distribution can therefore have a negative effect on the aerodynamic performance. The aerodynamic wing of the sailplane with morphing forward section has been designed and optimized by Achleitner et al [1]. Five different airfoils with a morphing forward section have been numerically optimized for minimum profile drag at relevant lift-coefficients and with regards to structural constraints and specific Reynolds numbers on the wing locations. The wing planform also has been optimized with the objective to minimize the difference between the induced drag coefficient and the induced drag coefficient of an elliptical circulation distribution. Elastic wing bending was considered by modifying the dihedral distribution with the result from a preliminary structural analysis without coupling. The result is a multi-trapezoidal planform with seven trapezoids and a rigid twist distribution to have the airfoils operate at the same zero lift angle of attack. Therefore, for this sailplane, the objective is chosen to minimize wing twist and therefore minimize the difference to the optimized aerodynamic design.

3.2 Structural Model

The structure of the wing is modeled by using a FE shell model covering the primary structure. This includes especially the torsion box, which is bounded by a main spar (box-beam for the inner wing and I-beam for the outer wing) and a c-shaped rear spar. The model was created from a simplified geometry, in which the shell is cut out in the area of the airbrake box and the flap control actuation

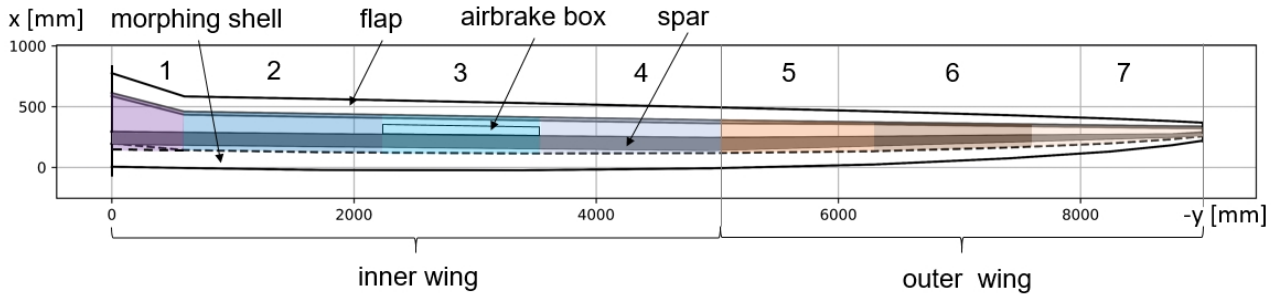

Figure 3 – Wing planform with seven design fields.

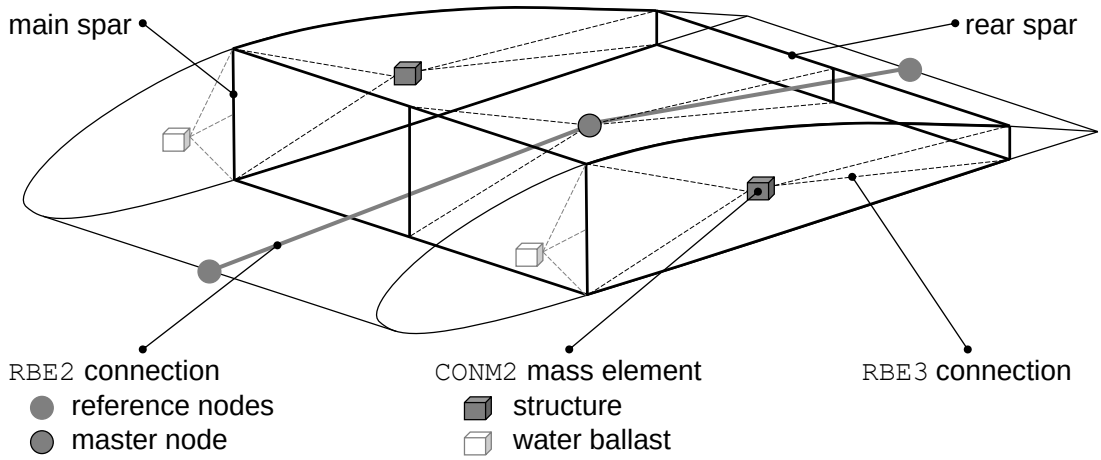

Figure 4 – Interface and mass model.

points. Different composite parts which overlap, such as the spar caps and the torsion shell, share the same elements in these areas. The element types chosen for the discretization are NASTRAN CQUAD4 and CTRIA3. Composite stiffness properties are defined by means of PCOMP property cards, which allows to assign ply thicknesses, orientations and materials. HM CFRP is predominantly used for the shell and the face sheets of the shear webs, whereas the main spar caps are made of HT CF rovings. Between main and rear spar, the shell is designed as a sandwich. Control surfaces do not contribute appreciably to the global stiffness and are therefore not modeled. Likewise, control rods are not considered. The morphing shell is also not modelled since it is not bonded to the skin on the lower side and therefore does not act as closed torsional cell.

Local reinforcements are provided in the area of the control cutouts and the airbrake box, where the structure is weakened. Likewise, there are UD reinforcement plies in the area of the root rib, both in the direction of flight and along the rear spar of the innermost trapezoid for load introduction from the fuselage.

Figure 3 shows the division of the wing structure into seven main design fields, four in the area of the inner wing and three more for the outer wing. Within these design fields, both orientations of single CFRP plies and overall layup thicknesses remain variable in order to exploit the anisotropy of the fibers efficiently for twist reduction.

The coupling of aerodynamic loads and structural deformations is realized by an interface model. Therefore, the structure is divided into 20 equidistant sections. Each section consists of three reference nodes, one located at the leading edge, one at the trailing edge and another at 60% chord. Structural deformations from these nodes are transferred to the aerodynamic model via SPLINE1 surface spline interpolation. Aerodynamic loads are returned to the coupling nodes and then trans-

ferred to the master node in the middle of each section via RBE2 rigid connections. From this master node, loads are introduced into the main and the rear spar via RBE3 interpolation elements, as shown in figure 4.
RBE3 elements can also be used for modeling structural parts that do not add artificial stiffness to the system. This includes masses in front and rear of the load carrying wing box like water ballast, morphing actuation and control system. The structural mass comprises the masses of all primary structure components. It can either be modeled by assigning densities to the material cards and calculating the overall mass by shell thicknesses, or by neglecting densities and adding a lumped mass distribution. The latter method is used to connect discrete CONM2 masses to the primary structure as figure 4 indicates. Water ballast can be modeled or omitted depending on the load case considered and the associated mass configuration as can be seen in figure 5.

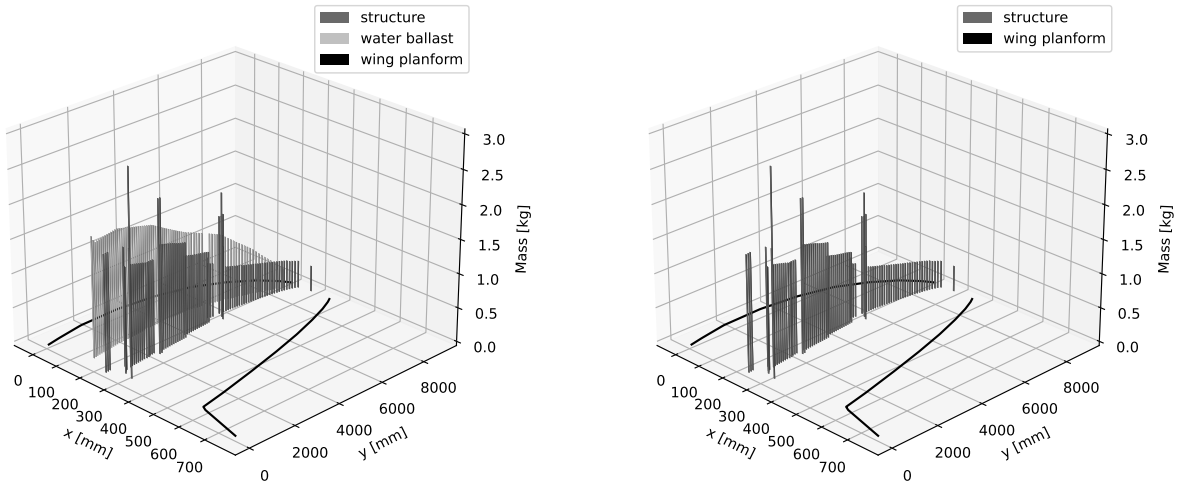

(a) water ballast included.

(b) water ballast omitted.

Figure 5 – Different mass configurations.

Figure 6 shows a section of the FE shell model in the inner wing area. In order to display the torsion box, the wing is cut at $y = 720$ mm. Clearly visible are structural cutouts in the area of the airbrake and the control actuation points. 1D elements (RBE2 and RBE3) for the aeroelastic interface and the mass model (hidden in this view, shown in figure 4) are connected to the displayed 2D elements. Leading and trailing edge of the wing are indicated as dashed lines, but do not count to the primary structure and are therefore omitted in the model.

3.3 Aerodynamic Model

The aerodynamic model is composed of a plane panel model, which represents the wing planform and a horizontal stabilizer for trimming, and a correction model, taking camber and twist information into account. Each trapezoid is described by its own CAERO1 panel, in which the number and spacing of small surface elements (boxes) can be defined in chordwise and spanwise direction separately. The $\frac{1}{4}$-chord line of each box contains a distributed acceleration potential doublet of uniform strength, describing the bound segment of a horseshoe vortex [2]. The box span becomes smaller towards the wing tip for an accurate representation of the boundary vortex. In flow direction, box lengths become smaller towards the leading edge and the trailing edge. NASTRAN W2GJ allows a rotation of the boxes local downwash vectors, thus adding camber and built-in twist to the flat panel model as figure 7 indicates. For each airfoil configuration a separate aerodynamic model is created. For the fast-flight configuration the forward section is unmorphed and the trailing edge flap is neutral. For the slow flight configuration, the forward section is morphed downwards and the trailing edge flap is also deflected downwards.

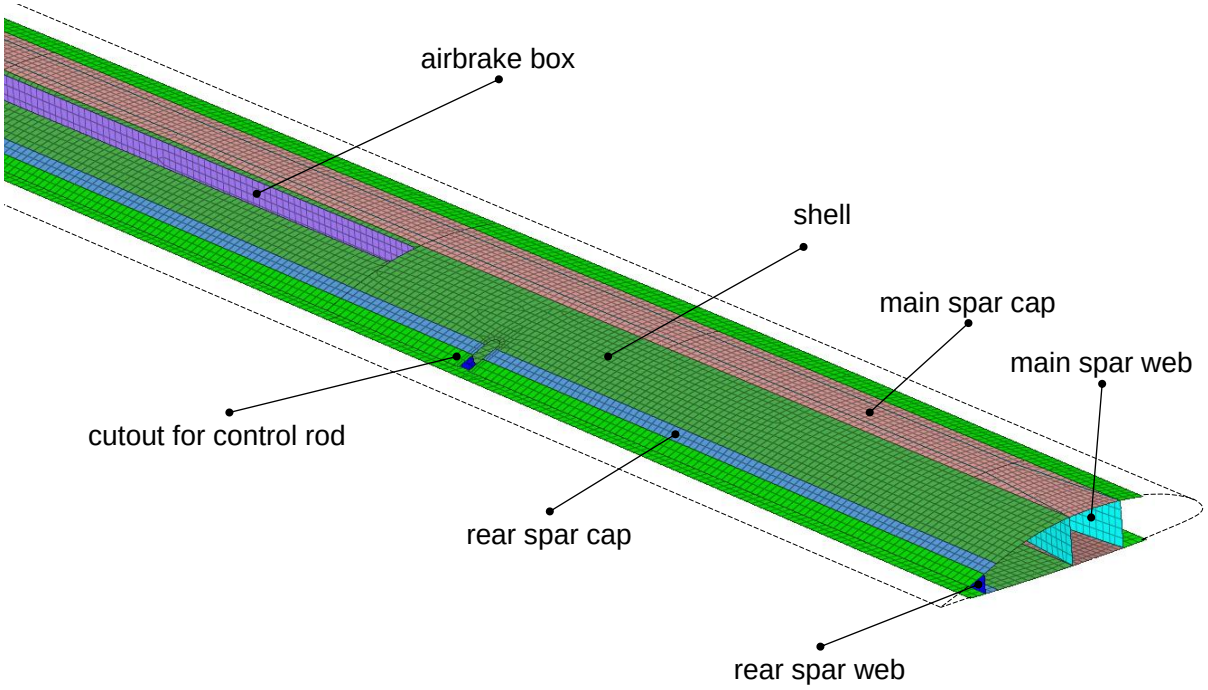

Figure 6 – FE shell model of the primary structure.

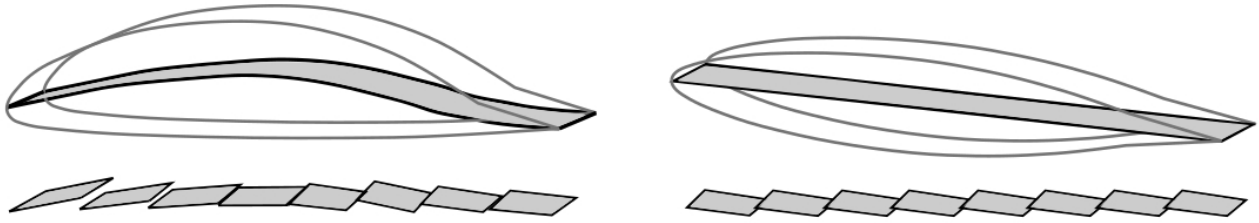

Figure 7 – Airfoil camber (left) and twist (right) correction of DLM boxes.

3.4 Aeroelastic Solution Sequence

Having generated structural, aerodynamic and mass model, they are combined for the `SOL144` static aeroelastic solution sequence. The aeroelastic model has two degrees of freedom for motion. One for plunging and one for pitching. Before running the simulation, input values for the dynamic pressure, the Mach number and the vertical acceleration are set. NASTRAN then performs a trim analysis and determines the global angle of attack for the converged flight condition [14]. The result comprises the aerodynamic and structural system response.

3.5 Optimization Approach

The optimization problem is to minimize the objective function z with upper and lower bounds for the design variables x. The design variables are used to modify ply angles and thicknesses directly in the NASTRAN input file. From the twist distribution, the objective function value is calculated.

$$\begin{aligned} &min\ (z(\vec{x})) \\ &subject\ to\ lb < \vec{x} < ub \end{aligned} \tag{1}$$

The laminate is modeled as a 90 ° cross-ply laminate, so two fiber directions are combined in a relative angle of 90 °. This is naturally the case for all woven-fabric plies. It can also be realized by combining UD plies. An advantage is, that the number of effective design variables for the laminate is reduced, as the second fiber angle is dependent on the first angle. The fiber orientation of the upper and lower wing shell is mirrored to achieve the desired coupling effect. Each shell laminate is modelled as a symmetrical sandwich in order to achieve a high buckling resistance compared to a

monolithic laminate. This is shown in figure 8. The thickness is treated a continuous design variable, although in reality only discrete thicknesses are available.

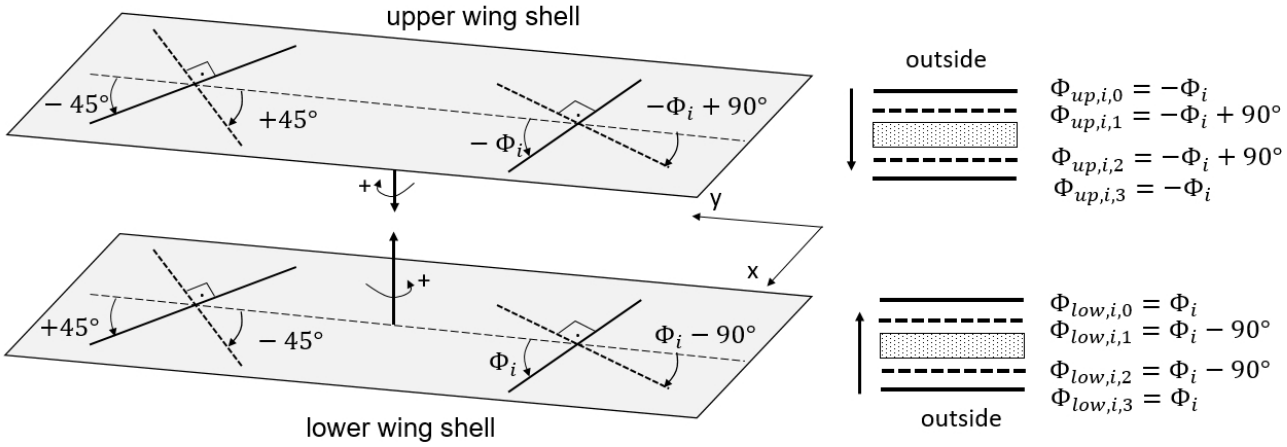

Figure 8 – Mirrored shell laminates with fiber angles.

The design variables x in equation 2 are one fiber angle θ and one thickness t per design field for n design fields on the wing. Several design fields can be grouped into a smaller number of global design fields, thus reducing the number of effective design variables. For example, design fields one to four could be grouped, so that the whole inner wing has the same layup. Furthermore, the design variable vector could contain exclusively angles or exclusively thicknesses.

$$\vec{x} = [\Phi_i, ..., \Phi_{n_{fields}}, t_i, ..., t_{n_{fields}s}]^T \tag{2}$$

The system responses from the solver are nodal deflections and rotations in the global $x-y-z$ coordinate system. A wing with bending deflection and the corresponding rotations is shown in figure 9 in the upper part. In the lower part, the displacements and rotation of an airfoil in the $x-z$ plane is shown. The twist angle θ is calculated with the difference of the deflections between leading edge and trailing edge nodes in equations 3 and 4. These are corrected with the local deformed dihedral angle γ in equation 5 to get the effective aerodynamic twist angle.

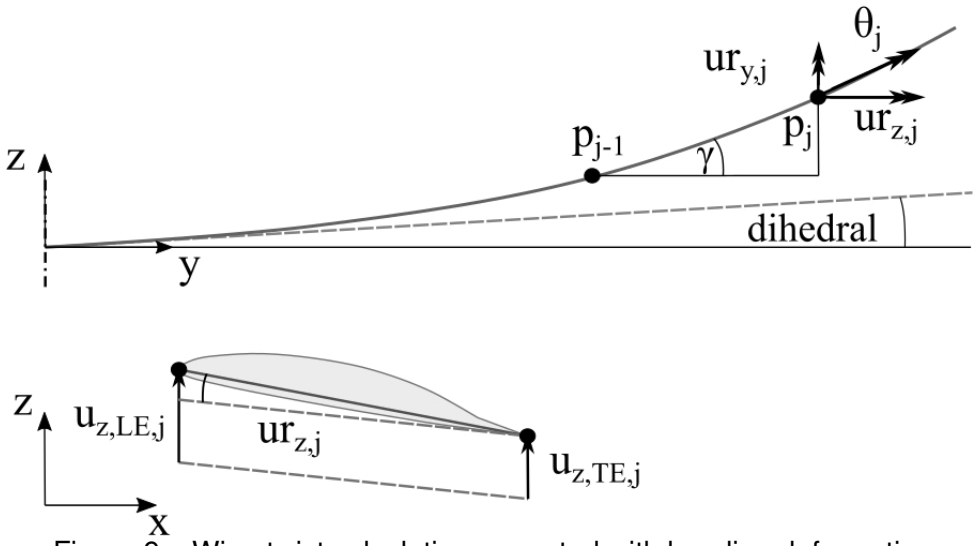

Figure 9 – Wing twist calculation corrected with bending deformation.

$$\theta_j = arctan(ur_{z,j}) \cdot cos(\gamma_j) + arctan(ur_{y,j}) \cdot sin(\gamma_j) \tag{3}$$

$$\theta_j = arctan(\frac{u_{z,LE,j} - u_{z,TE,j}}{u_{x,TE,j} - u_{x,LE,j}}) \cdot cos(\gamma_j) + arctan(\frac{u_{y,TE,j} - u_{y,LE,j}}{u_{x,TE,j} - u_{x,LE,j}}) \cdot sin(\gamma_j) \tag{4}$$

$$\gamma_j = arctan(\frac{z_{mid,j} - z_{mid,j-1}}{y_{mid,j} - y_{mid,j-1}}) \tag{5}$$

The objective function formulation as proposed by Schlothauer [18] is used. The objective function value z in equation 6 is the sum of all squared rotation angles along discrete spanwise locations, summed up with a weight factor for all load cases. By this, both positive and negative angles contribute to the objective function the same way.

$$z(\vec{x}) = \sum_{k}^{n_{LC}} (w_k * \sum_{j}^{n_{nodes}} (\theta_{j,k})^2) \tag{6}$$

The design variables are normalized from the physical variables in equation 7 and equation 8. So they take a value from 0 to 1 within the range of lower bounds lb and upper bounds ub. In this case, the values for fiber angle are on order of magnitude higher than those of the thickness. The normalization of all design variables shows benefits for a quicker convergence of the optimization algorithm.

$$x_i = \frac{x_{phys,i} - lb_{phys,i}}{ub_{phys,i} - lb_{phys,i}} \tag{7}$$

$$x_{phys,i} = lb_{phys,i} + x_i \cdot (ub_{phys,i} - lb_{phys,i}) \tag{8}$$

The bounds for the fiber angles are set to 35 ° and 55 °. Although the theoretical range reaches from 0 ° to 90 °, values outside the bounds lead to significantly adverse wing twists.
The ply thicknesses are allowed to vary from 0.3 mm to 0.8 mm, so here bounds are implemented for the thickness design variables.
The optimization algorithm Sbplx implemented in NLopt was used [11]. It is based on the Subplex method by Rowan [8] which is a gradient-free method for unconstrained problems based on the Nelder-Mead simplex algorithm [15]. The algorithm uses Nelder-Mead on a sequence of subspaces, promises to be more robust than the original and can handle bounds. An implementation of COBYLA (Constrained Optimization BY Linear Approximations) by Powell [16] in NLopt tended to run into local minima for these kind of optimization problems. The optimization workflow is shown in a flowchart in figure 10.

3.6 Load Cases and Mass Configurations

Six representative load cases are selected. They comprise two cruise cases in fast-flight configuration (airfoil config 0) and two thermaling cases in slow-flight configuration (airfoil config 1) that are used for combined optimization, each with a weight factor of $w_k = 0.25$. In addition there are two pull-up load cases at maneuver speed. They are not used in the optimization loop, but only for analysis after the optimization. For the fast-flight airfoil configuration a load factor of $n_z = 3.0$ is used, for the slow-flight configuration the load factor is $n_z = 5.6$. The cases are listed in table 1.
Three mass configurations are considered. MC 1 is a configuration with maximum take-of mass, that is realized with a total of 193 kg water ballast in the wing, which almost doubles the wing mass compared to the empty configuration. To reduce trim drag, a center of gravity position at 73 % of the allowable range is created by additional water ballast in the vertical stabilizer. MC 2 has no water ballast and therefore a significantly lower take-off weight. They represent typical competition loading configurations for strong and weak thermal conditions. MC 3 is a mass configuration with maximum take-off weight that leads to the highest root bending moments. Therefore the maximum mass of the non-lifting parts and a forward center of gravity is applied. In general, water ballast in the wings does not increase the root bending moment more, compared to adding the same mass in the non-lifting parts. In this model, ply thicknesses have no effect on mass as the used materials have no assigned densities. Since the operational spectrum of a sailplane covers a wide range of take-off masses, namely from the lowest take-off mass without water ballast to MTOM including water ballast, the effects of the selected mass configurations in combination with the selected load cases are investigated. This also serves to assess the influence of mass distribution along the span, but also

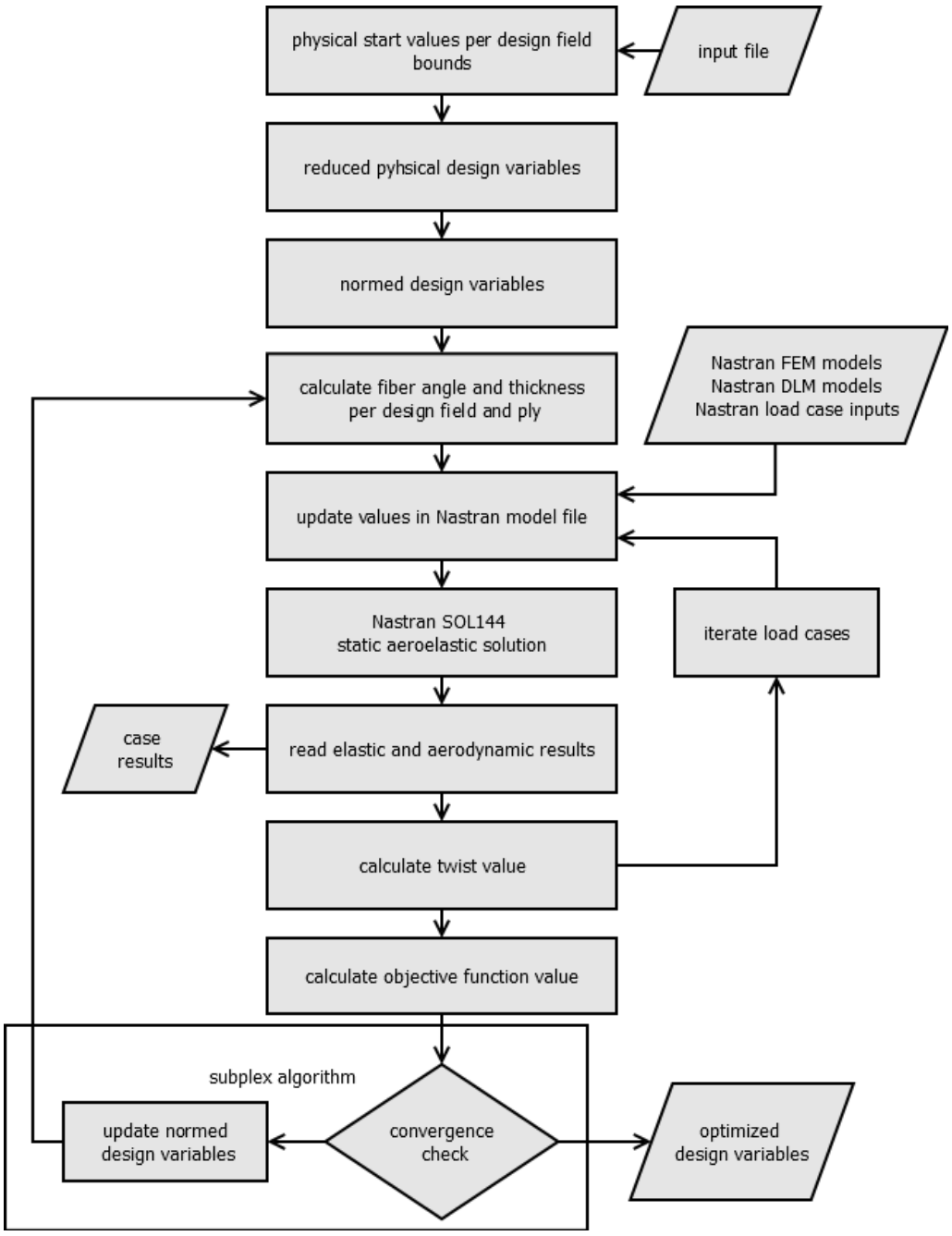

Figure 10 – Optimization workflow.

along the chord, since the water ballast is placed in the wing's forward section and thus generates a restoring moment that counteracts wash-in.

Table 1 – List of selected load cases with weight factors.

LC ID	Description	Airfoil Config	MC ID	$n_z\ [-]$	$V\ [km/h]$	$C_L\ [-]$	$w_k\ [-]$
0	Cruise, unmorph	0	1	1.00	220	0.30	0.25
1	Cruise, unmorph, no water	0	2	1.00	220	0.20	0.25
2	Thermaling, morph	1	1	1.30	110	1.54	0.25
3	Thermaling, morph, no water	1	2	1.41	90	1.67	0.25
4	Pull-up, unmorph	0	3	3.00	220	0.89	-
5	Pull-up, morph	1	3	5.30	220	1.57	-

Table 2 – List of mass configurations.

MC ID	Description	$m\ [kg]$	$m_{NL}\ [kg]$	$m_{S,wing}\ [kg]$	$m_{WB,wing}\ [kg]$	$x_{CG,allow}\ [-]$
1	Competition, water	600	210	197	193	0.73
2	Competition, no water	402	205	197	0	0.73
3	MTOM, max bend, forward CG	600	300	197	103	0.00

4. Results

First optimization studies are done with single load cases and one design field (whole wing) to clearly examine the influence of the design variables on the objective function value. In figures 11 and 13 the results of the optimization run are shown for one design field, so there is one fiber angle ϕ and one thickness t. For LC 3 in figure 11 the objective function value is minimized in a narrow band of fiber angles, with a minimum at the lower bound thickness of $t_{opt,LC3} = 0.3$ mm and $\phi_{opt,LC3} = 46.5\ ^\circ$. The sensitivity with regard to the fiber angle however is much higher than to the ply thickness. Similar results can be seen for all other single load cases.

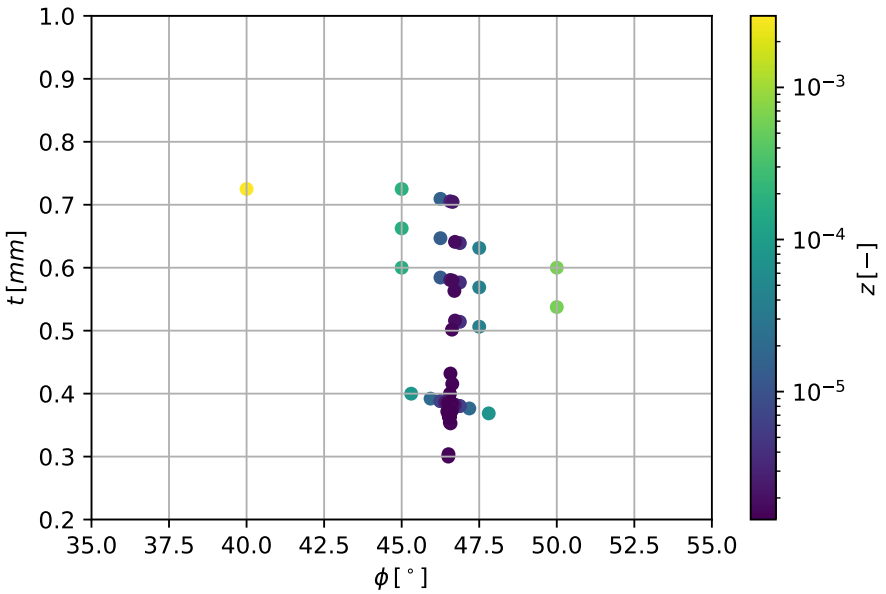

Figure 11 – Design space during optimization with single LC 3, one design field.

For LC 0, 1, 2, 3 combined with a weighted sum objective function value, the design variables are shown in 12. The sensitivity with regard to the fiber angle still is much higher than to the thickness. The optimum thickness converges at the upper bound of $t_{opt,all\,LCs} = 0.8$ mm. The optimum angle is at $\phi_{opt,all\,LCs} = 46.6\ ^\circ$.
For LC 0 and the combined cases the optimum thickness is at the upper bound thickness of $t_{ub} = 0.8$ mm, for the other single cases, the optimum thickness is lower. Comparing to the start value for the angle $\phi_0 = 45.0\ ^\circ$, all optimum angle values increase and lead to a wash-out twist, except for LC 2 and LC 5. All optimized design values for one design field are plotted in figure 13.

In the second part of the study, all design load cases have been considered with their corresponding weight factors of 0.25. Now the influence of the number of design fields on the result is analyzed. In the case of two design fields, all four fields of the inner wing are combined and all three fields of the outer wing are combined as well. The optimized fiber angles are:

$$\phi_{opt,2DF} = [46.8^\circ, 45.7^\circ]^T \tag{9}$$

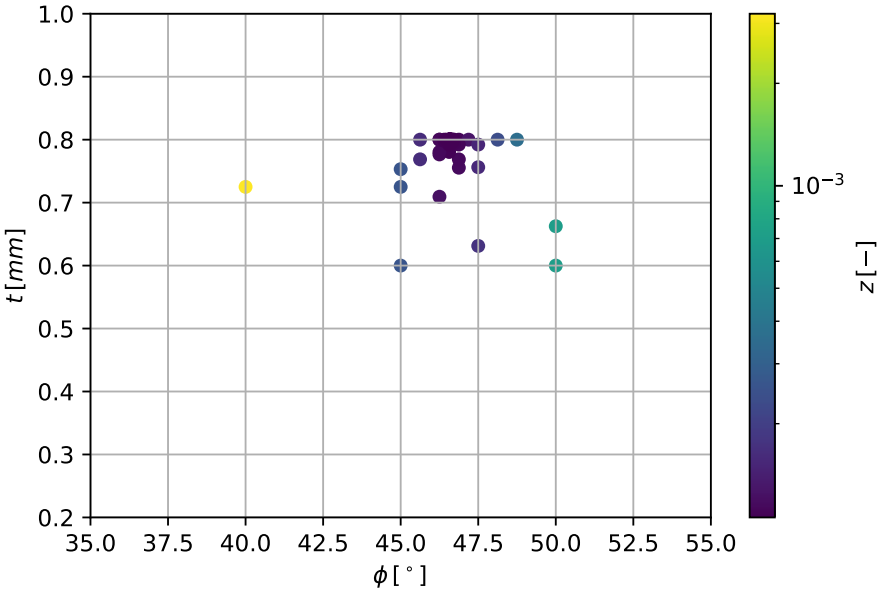

Figure 12 – Design space during optimization with LC 0,1,2,3, one design field.

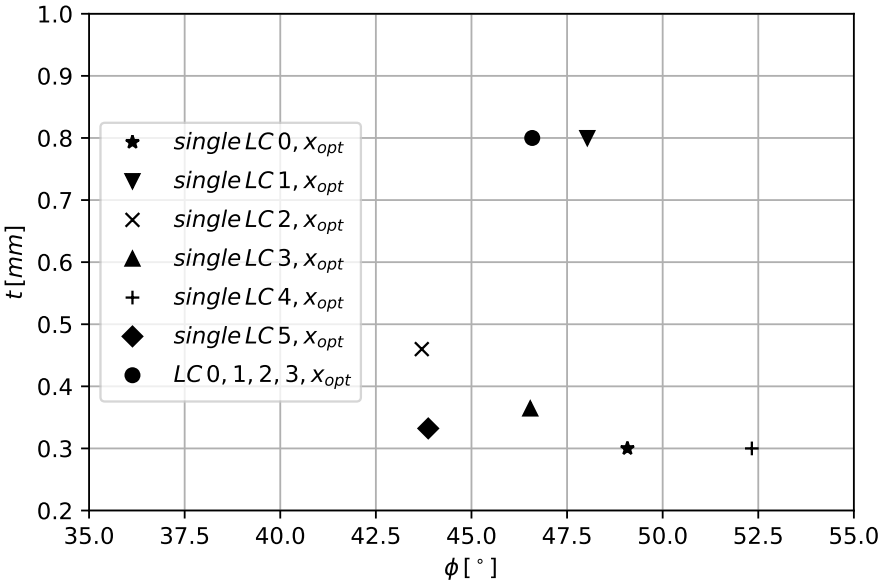

Figure 13 – Optimized design variables for single and combined load cases and one design field.

The thicknesses converge at the upper bound of 0.8 mm.
For seven design fields, the optimized fiber angles are:

$$\phi_{opt,7DF} = [42.9°, 47.8°, 46.2°, 47.6°, 45.7°, 45.8°, 43.4°]^T \tag{10}$$

Locally the fiber angles are above the start values of $45.0°$, except for the inner- and outermost trapezoid of the wing. The thicknesses all converge at the upper bound of 0.8 mm.
In figure 14 the wing twist ϕ over spanwise coordinate y is shown for LC 0. At the start values there is a wash-in twist due to the aft position of the elastic axis compared the the aerodynamic center. The twist has been reduced by the optimization. There are kinks in the distribution that can be traced back to the airbrake box cutout and the transition from inner to outer wing. For LC 0 and one design field there is less twist in the outer wing area comparing to two design fields.

For LC 1 in figure 15, the result looks similar to LC 0, however there is less initial twist. The difference

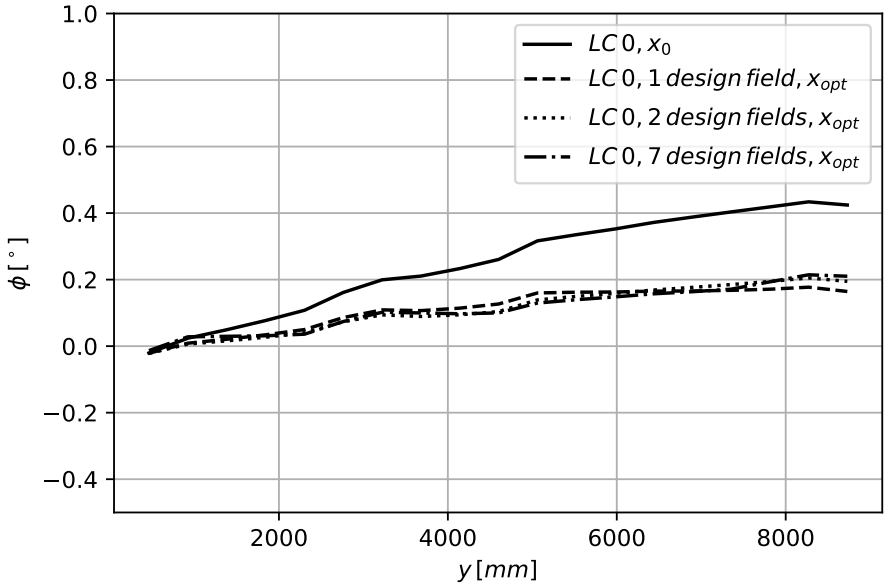

Figure 14 – Optimized twist distribution LC 0.

in twist between the start design and the optimized design is in a comparable range for LC 0 and LC 1, despite a significant difference in wing mass.

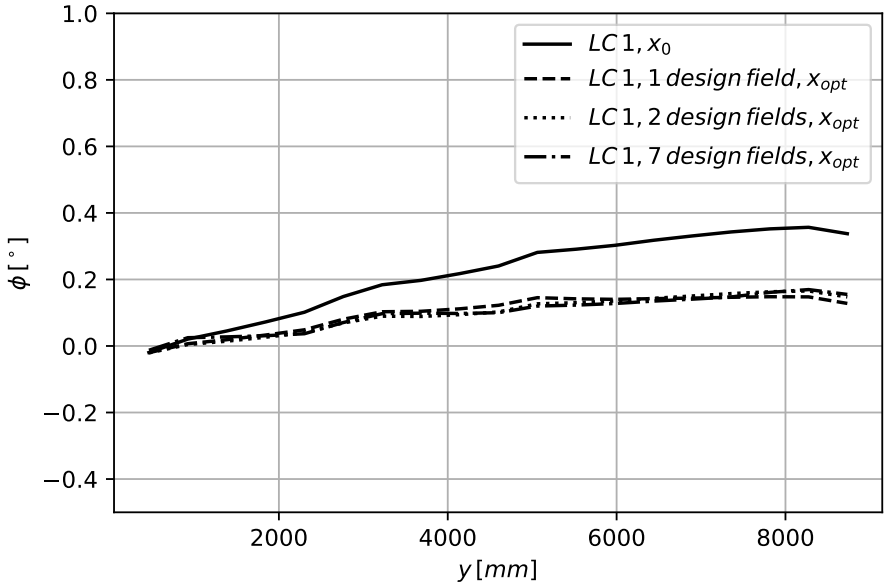

Figure 15 – Optimized twist distribution LC 1.

The twist distributions for the optimized design variables analyzed at LC 2 are shown in figure 16. The initial twist distribution already has a negative wash-out twist due to the airfoil pitching moment in slow flight configuration. The bending torsion coupling from the optimized design variables leads to an adverse twist effect with higher negative twist angles for this case. The results for LC 3 look similar to those of LC 1 and LC 2.

The bending deflections for LC 0 and LC 2 are shown in figure 17 for the start design and the optimized design with one design field. The deflection on the vertical axis is scaled with a factor of ten compared to the horizontal axis to better display the differences. The absolute deflection differences between the two load cases is low, so the different torsion signs of the initial designs for LC 0 and LC 2 are not created by bending torsion coupling but airfoil pitching moments.

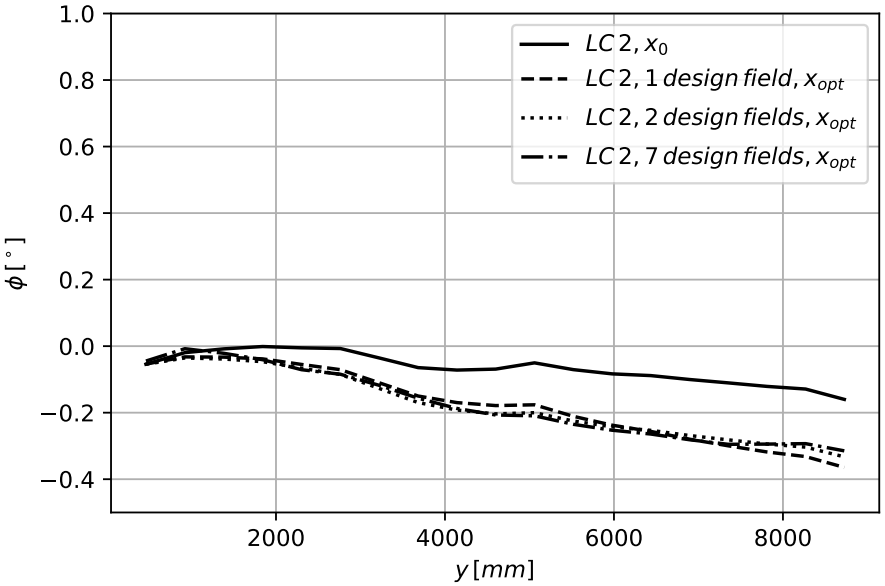

Figure 16 – Optimized twist distribution LC 2.

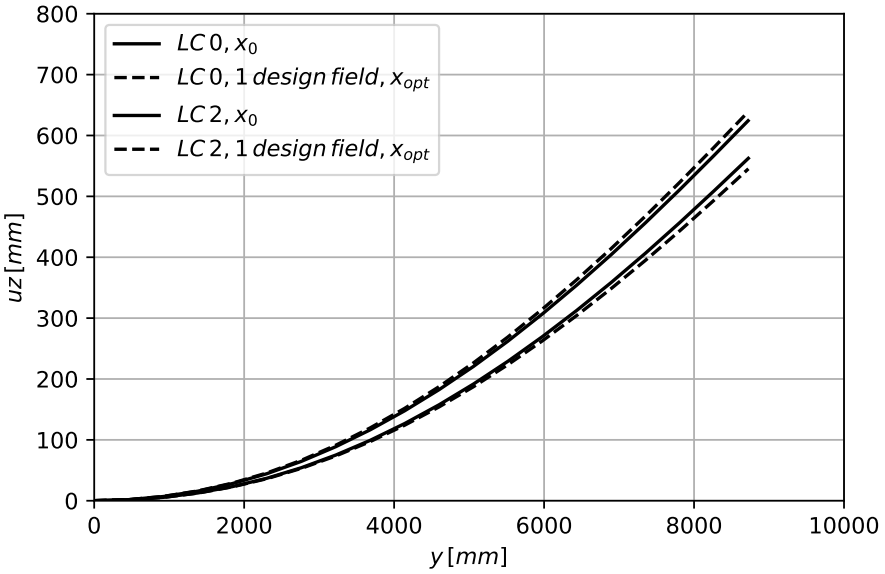

Figure 17 – Bending deflection of LC 0 and LC2.

For the pull-up maneuver load cases the twist distributions are shown in figure 18. Initially there is a significantly higher twist for LC 4 compared to all other cases over the whole wing. With the optimized design variables the twist can be significantly reduced. For LC 5 the start design already has a wash-out effect that is increased by bending torsion coupling after optimization.

In figure 19 the local lift coefficients are plotted for LC 0 and LC 4 and two design fields. For LC 0 and LC 4 the wash-out effect on twist leads to a lift coefficient increase towards the root and to a reduction towards the wing tip for a trimmed flight condition. A more even lift distribution leads to reduced induced drag and the inward shift of lift leads to a load alleviation effect and a reduced root bending moment, especially for pull-up maneuver load cases.

In the third part of the study, optimization was performed only for load cases LC 0 and LC 1 (cruise flight) with weight factors of 0.5, the twist can be further reduced. However, in the thermal load cases,

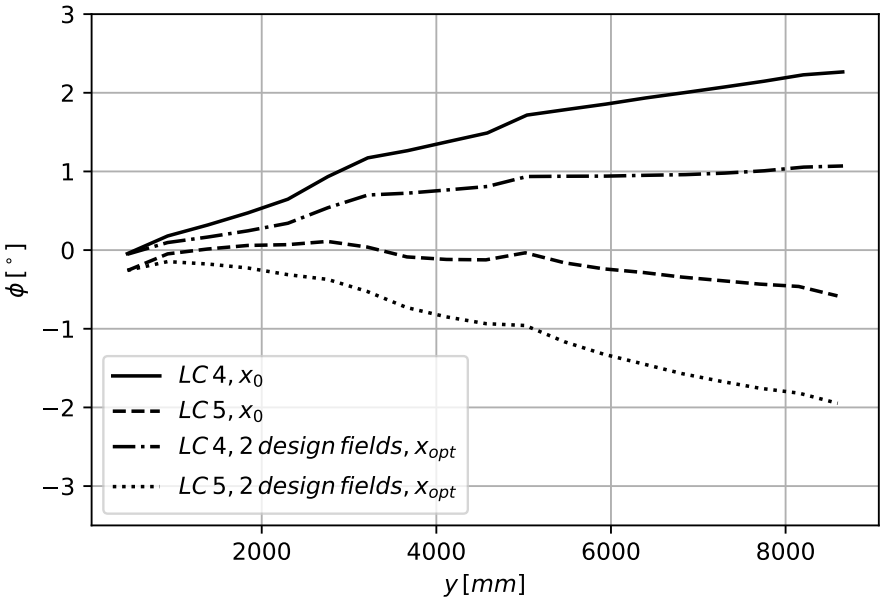

Figure 18 – Twist distributions LC 4 and LC 5.

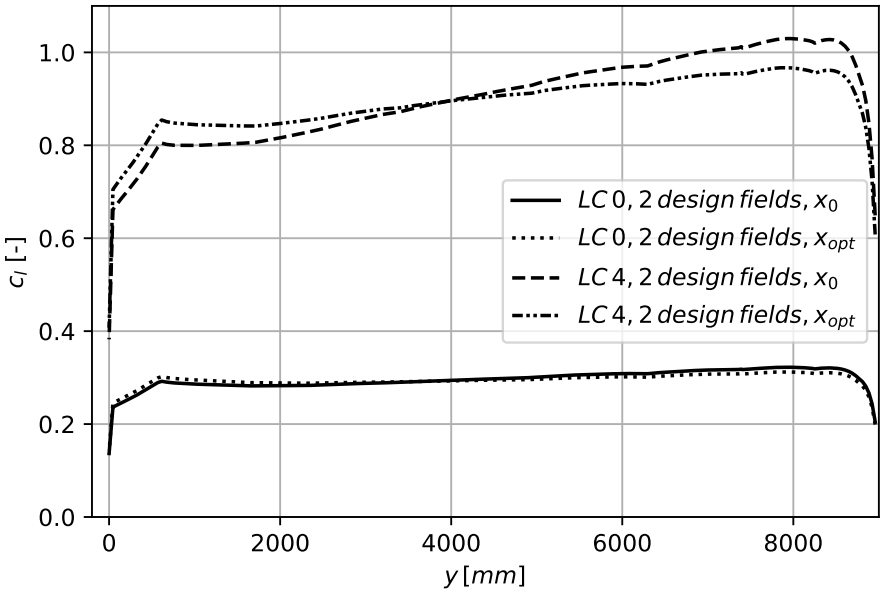

Figure 19 – Local c_l lift coefficient distributions for LC 0 and LC 4.

the twist is increased. The resulting fiber angles for two design fields are:

$$\phi_{opt,2DF,cruise} = [48.7°, 47.4°]^T \tag{11}$$

The fiber angles are higher compared to those in formula 10 for the optimization with LCs 0, 1, 2, 3. Then the optimized thicknesses converge no longer at the upper bound value, but at a smaller value, which is also adverse for those load cases that have not been considered in the objective function.

$$t_{opt,2DF,cruise} = [0.56\,mm, 0.48\,mm]^T \tag{12}$$

Convergence of an optimization run is reached in the order of 50 to 500 iterations, depending on the number of effective design variables. On a current workstation PC the aeroelastic solution of one load case takes in the order of 30 seconds.

5. Conclusion and Outlook

A method for static aeroelastic tailoring to reduce twist of aircraft wings has been developed and applied to a high-aspect-ratio wing of a sailplane with a morphing forward section. The approach is to directly modify fiber angles and thicknesses of a FE shell model and to combine physical design variables to a reduced set of effective design variables. The method is efficient in terms of modelling for a wing design with a fixed aerodynamic hull and in terms of computational effort.

The investigations show that wing twist can be reduced by applying bending-torsion coupling. The effect of the fiber angle is much more dominant compared to the stiffness influence from laminate thickness. Looking at one design field and optimizations of single load cases, the minimum twist is achieved in a narrow band of fiber angles and does not change much in the whole range of bound thicknesses. For several single load cases with one design field the objective function values are lower for the smallest allowed thickness. As the torsional stiffness of the examined wing changes in spanwise direction due to the geometry, the coupling effect is only beneficial in some areas of the wing and adverse in other areas. Therefore, less absolute stiffness leads to a slightly better result. Each load case separately leads to one optimum fiber angle, the absolute difference of the angles is less than 10 $^\circ$ and twists the wing tip in the order of 2 $^\circ$ for pull-up load cases.

With more than one design field and more than one load case, the optimum stiffness converges at the upper bound. In the case of the investigated sailplane the airfoil configuration (fast-flight, slow-flight) has a large influence on the airfoil pitching moment and therefore wing twist. In the morphed configuration there is already a wash-out effect for the start design. Here, the bending-torsion coupling due to aeroelastic tailoring leads to an adverse effect on the twist distribution. However, this can be beneficial for high load factors as it leads to a load alleviation effect. The actual result of the optimization depends on the weight factors of the load cases, as the bending-torsion coupling in one direction is either beneficial or adverse, depending on the case. However, an absolute high torsional stiffness, for example by using a high ply thickness or a material with a high Young's modulus, is beneficial in every case.

By using more than one design field, a more even twist distribution can be achieved, especially for wings with significant geometric changes in spanwise direction. The absolute effect on the result however leads to a more complex fiber layout. In this specific case the tailored fiber angles vary in the order of 5 $^\circ$ which requires high manufacturing accuracy. Based on the presented approach, the influence of the changing mass distribution, calculated by material densities, due to varying optimized thicknesses can be investigated in further studies. Furthermore, the effect of independent fiber angles on the result can be researched. By coupling the aerodynamic response with a geometric nonlinear FE solution, buckling can be examined and large bending deflections for pull-up load cases can be regarded. The method can be applied for other wing configurations, with and without a morphing wing section. In the case of a morphing forward section, the stiffness of the compliant mechanism ribs can be incorporated to include the stiffness of the morphing shell.

6. Acknowledgment

The present studies have been funded under the grant of the German federal aviation research program LuFo V-3 (Luftfahrtforschungsprogramm V-3). The authors would like to acknowledge the support of the German Federal Ministry for Economic Affairs and Energy.

7. Contact Author Email Address

fabian.sturm@tum.de

8. Copyright Statement

References

[1] Achleitner, J., Rohde-Brandenburger, K., Rogalla von Bieberstein, P., Sturm, F., and Hornung, M. Aerodynamic Design of a Morphing Wing Sailplane. In *AIAA Aviation 2019 Forum*, page 4, Reston, Virginia, 06172019. American Institute of Aeronautics and Astronautics.

[2] Albano, E. and Rodden, W. P. A Doublet-Lattice Method for Calculating Lift Distributions on Oscillating Surfaces in Subsonic Flows. *AIAA Journal*, 7(2):279–285, 1969.

[3] Boermans, L.M.M. Research on Sailplane Aerodynamics at Delft University of Technology. *Technical Soaring*, (Vol. 30, No.1/2), 2006.

[4] Boermans, L.M.M. On the Way to Glide Ratio 100:1. In R. Radespiel and T. Landa, editors, *XXXIV OSTIV Congress*, pages 107–110. TU Braunschweig Niedersächsisches Forschungszentrum für Luftfahrt, Braunschweig, 2018.

[5] Dillinger, J. K. S. Static Aeroelastic Optimization of Composite Wings with Variable Stiffness Laminates. Dissertation, 2014.

[6] Dillinger, J. K. S., Abdalla, M. M., Meddaikar, Y. M., and Klimmek, Thomas. Static Aeroelastic Stiffness Optimization of a Forward Swept Composite Wing with CFD-Corrected Aero Loads. *CEAS Aeronautical Journal*, 10(4):1015–1032, 2019.

[7] European Aviation Safety Authority. Certification Specifications for Sailplanes and Powered Sailplanes CS-22: Amendment 2, 2009.

[8] Harvey Rowan, T. Functional Stability Analysis Of Numerical Algorithms. Technical report, 1990.

[9] IJsselmuiden, S. T. Optimal Design of Variable Stiffness Composite Structures using Lamination Parameters. Master's thesis, 2011.

[10] Illenberger, G. M. Numerical Investigations on the Static Aeroelasticity of a Sailplane with a Morphing Forward Wing Section. Semesterarbeit, Technical University of Munich, 2019.

[11] Johnson, S.G. The NLopt Nonlinear-Optimization Package, 2021.

[12] Karaolis, N.M., Mussgrove, P.J., and Jeronimidis, G. Active and Passive Aeroelastic Power Control Using Asymmetric Fibre Reinforced Laminates for Wind Turbine Blades. In *Proceedings of the 10th British Wind Energy Conference, London*, pages 446–458, 1988.

[13] Lobitz, D., Veers, P., Eisler, G., Laino, D., Migliore, P., and Bir, G. The Use of Twist-Coupled Blades to Enhance the Performance of Horizontal Axis Wind Turbines. 01 2001.

[14] MSC. *Aeroelastic Analysis User's Guide*. MSC Software, 2004.

[15] Nelder, J.A. and Mead, R. A Simplex Method for Function Minimization. *Computer Journal*, 7:308–313, 1965.

[16] Powell M. J. D. Direct Search Algorithms for Optimization Calculations, 1998.

[17] Reinisch, J., Wehrle, E., and Achleitner, J. Multiresolution Topology Optimization of Large-Deformation Path-Generation Compliant Mechanisms with Stress Constraints. *Applied Sciences*, 11(6):2479, 2021.

[18] Schlothauer, A. Strukturelle Auslegung und Aeroelastic Tailoring eines Segelflugzeug Tragflügels mit formvariabler Vorderkante. Semesterarbeit, Technical University of Munich, 2016.

[19] Shirk M. H., Hertz T. J., and Weisshaar T. A. Aeroelastic Tailoring - Theory, Practice, and Promise. *Journal of Aircraft*, 23(1):6–18, 1986.

[20] Sturm F., Achleitner J., Jocham K., and Hornung M. Studies of Anisotropic Wing Shell Concepts for a Sailplane with a Morphing Forward Wing Section. In *AIAA Aviation 2019 Forum*, page 4, Reston, Virginia, 06172019. American Institute of Aeronautics and Astronautics.

[21] T. N. van den Bosch. The aeroelastic Tailoring of a High Aspect Ratio Composite Structure.

[22] Vanderplaats, G. N. and Weisshaar, T. A. . Optimum Design of Composite Structures. *International Journal for Numerical Methods in Engineering*, 27(2):437–448, 1989.

[23] Weinzierl, M., Achleitner, J., and Baier, H. Highly Extensible Skin of a Variable Geometry Wing Leading Edge of a High-Performance Sailplane. *Technical Soaring*, (Vol. 39, No. 1):4–9, 2015.